Styrene Maleic Anhydride Copolymer Mediated Dispersion of Single Wall Carbon Nanotubes in Polyamide 12: Crystallization Behavior and Morphology

Arup R. Bhattacharyya,[1] Suryasarathi Bose,[1] Ajit R. Kulkarni,[1] Petra Pötschke,[2] Liane Häußler,[2] Dieter Fischer,[2] Dieter Jehnichen[2]

[1]*Department of Metallurgical Engineering and Materials Science, Indian Institute of Technology Bombay, Powai, Mumbai 400076, India*
[2]*Leibniz Institute of Polymer Research Dresden, D-01069 Dresden, Germany*

Received 29 January 2007; revised 28 March 2007; accepted 29 March 2007
DOI 10.1002/app.26680
Published online 15 June 2007 in Wiley InterScience (www.interscience.wiley.com).

ABSTRACT: Melt mixed composites based on polyamide 12 (PA12) were prepared using single wall carbon nanotubes (SWNT), which were encapsulated by styrene maleic anhydride copolymer (SMA). The aim was to achieve a reactive coupling between the maleic anhydride functionality of SMA at the surface of the SWNT and the amine end groups of PA12 during the melt mixing. The reaction could be proven by infrared spectroscopy. The modified nanocomposites exhibited a better SWNT dispersion. An enhanced interfacial adhesion between PA12 and SWNT was detected from SEM investigations of tensile fractured surfaces of the SMA encapsulated PA12/SWNT composites. Electrical conductivity measurements revealed the formation of ''network-like'' structure formation at 6 wt % SWNT content in PA12/SWNT composites, however, PA12/SWNT + SMA composites showed insulating behavior due to encapsulating SMA layer on SWNT surface. Studies on crystallization behavior indicated the nucleating action of unmodified and SMA encapsulated SWNT in the respective composites as found in the increase of crystallization temperature and the change in the crystalline morphology of PA12 as observed from DSC, WAXD, and SAXS. However, the degree of crystallinity of PA12 increased only marginally on incorporation of either unmodified or SMA encapsulated SWNT. © 2007 Wiley Periodicals, Inc. J Appl Polym Sci 106: 345–353, 2007

Key words: single wall carbon nanotubes; polyamides; reactive coupling; morphology; crystallization

INTRODUCTION

Since Iijima announced his discovery of carbon nanotubes (CNT) using high resolution TEM in 1991,[1] potential application areas of this nano-material having extraordinary mechanical, electrical, and thermal properties have attracted much attention toward industrial and research community.[2,3] Exemplary evidences are reported for single wall carbon nanotubes (SWNT) or multiwall carbon nanotubes (MWNT) based polymer composites, which includes PS/MWNT, PMMA/SWNT, PP/SWNT, PBO/SWNT, PVA/SWNT, PVA/MWNT, epoxy/MWNT, and PA12/MWNT.[4–12] Even if potential benefits associated with CNT have been confirmed, uniform dispersion of CNT still remains a challenge in exploiting the exceptional properties of CNT. Next to homogeneous dispersion adequate interfacial adhesion is found to be a key parameter for achieving superior mechanical properties in CNT/polymer composites.

Several routes were adopted to minimize the interfacial tension between the polymer matrix and the CNT to enhance dispersion and interfacial adhesion, which include the use of nonionic surfactants, the use of amphiphilic molecules such as palmitic acid, use of functionalized CNT, use of organic modifier with ionic moieties, and use of encapsulating polymer layer in CNT/polymer composites.[13–20] Further, enhanced dispersion of either SWNT/MWNT was reported by utilizing specific interaction of ''cation-π'' type between π electron clouds of CNT and cation containing organic modifier.[19,21] In addition, reactive coupling was shown to be a dominant factor besides ''cation-π'' interaction in controlling the dispersion of MWNT in PA6 matrix.[19]

In one of our previous communications, a novel approach of utilizing styrene-maleic-anhydride copolymer (SMA) encapsulated SWNT was reported to promote interfacial reaction between polyamide 12 (PA12) and SMA modified SWNT during melt processing to achieve better SWNT dispersion.[22] Further, the concept of reactive coupling was studied in melt-mixed composites based on polyamide 6 and SWNT.[23,24]

Correspondence to: A. R. Bhattacharyya (arupranjan@iitb.ac.in).

Contract grant sponsor: Leibniz Institute of Polymer Research Dresden.

Journal of Applied Polymer Science, Vol. 106, 345–353 (2007)

The advantage of reactive compatibilization lies in its simplicity and applicability for industrial nanocomposite production as well. Direct chemical modification of the nanotubes often leads to detrimental effect in connection with the structural integrity of the nanotubes, which is otherwise also not suitable for companies compounding fillers into polymers due to enhanced production cost associated with modification. The encapsulation of the nanotubes by SMA is easy to achieve and incorporation into the matrix polymer can be done in common melt-mixing equipments, like extruders.

This work attempts to understand the role of reactive compatibilization and the induced improved dispersion of SWNT on the crystallization behavior of PA12. Further, AC electrical conductivity measurements and morphological characterization were performed to assess the state of SWNT dispersion, ''network-like'' structure formation, and interfacial adhesion associated with encapsulation phenomenon.

Further, the focus of this work was based on an industrially available SWNT material. We have to take into account that the purity level of this specific SWNT batch was not very high, but typical for SWNT materials produced by arc discharge method. To evaluate the performance of a typical composite system with industrial grade SWNT we did not perform any additional (cost intensive) purification steps.

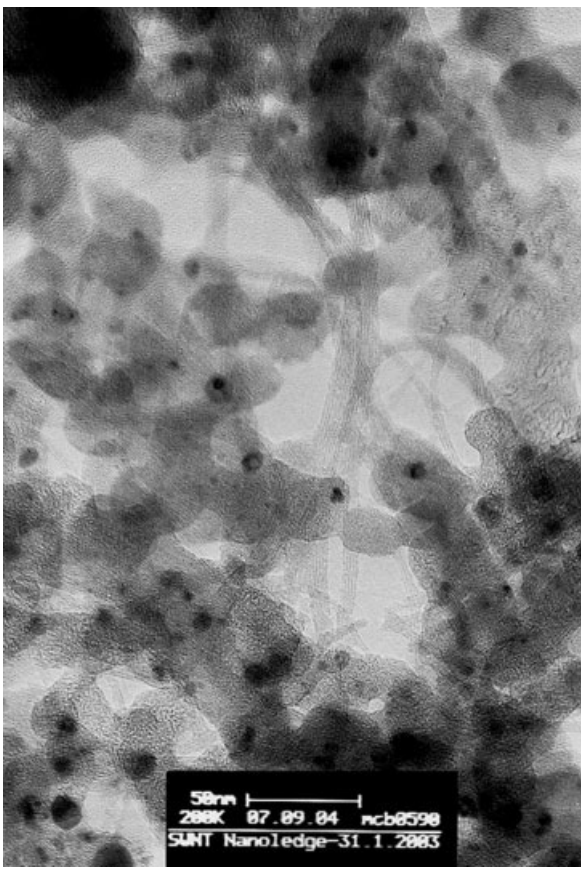

Figure 1 Transmission electron micrograph of the SWNT material as received.

EXPERIMENTAL

Materials and composite preparation

The SWNT material (obtained from Nanoledge S.A, France) was produced by electric arc discharge method and had a purity of about 55%. Transmission electron micrograph of the SWNT (Fig. 1) shows that it consists of a mixture of SWNT bundles (7–10 tubes), catalyst particles, and different types of graphene. The SWNT have a mean diameter of 1.33 ± 0.1 nm and length ranging from 2 to 5 μm (according to the supplier).

The PA12 used in this study had a melt flow rate of 154 g/10 min (275°C, 5 kg). ^{1}H NMR indicated nearly equivalence of NH_2 and COOH end groups and a degree of polymerization of about 60. The styrene maleic anhydride copolymers (SMA, supplied by NOVA Chemicals Corp.) were Dylark 232 (SMA8) and Dylark 332 (SMA14) where the MA levels were 8 and 14%, respectively.

The SMA modified SWNT were prepared by dissolving 0.042 g SMA in 50 mL tetrahydrofurane (THF) solvent utilizing ultrasonicator aided dispersion of SWNT (0.126 or 0.252 g, respectively) for 15 min and subsequently forming a ''mat'' by solvent removal. Unmodified SWNT were treated in the same way. The composites were prepared by melt mixing unmodified SWNT and SMA modified SWNT with PA12 powder in a conical twin-screw extruder (DACA Micro Compounder, capacity 4.5 cm^3) at 220°C with a rotational speed of 50 rpm for 15 min. The SWNT contents were 3 and 6 wt %. In case of SMA modified SWNT composites, SMA concentration was kept at 1 wt %. Prior to mixing the materials were dried for 24 h at 80°C in a vacuum oven. From a portion of the extruded strands sheets with a thickness of 0.35 mm were pressed using a Vogt press at 220°C.

Characterization methods

Attenuated Total Reflection (ATR) spectra were measured with an IR spectrometer IFS66v (BRUKER OPTICS, Germany) and the ''Golden Gate'' ATR cell (SPECAC, UK) in the wavelength range between 600 and 4000 cm^{-1} and a MCT detector with 100 accumulations and a resolution of 4 cm^{-1}.

The AC conductivity measurements were performed on the compression molded samples (across the thickness) in the frequency range between 10^{-2}

and 10^7 Hz using Alpha high-resolution analyzer coupled to a Novocontrol interface (broad band dielectric converter). The samples were placed between the two gold electrodes that were pressed together with a screw. The DC conductivity of the samples was determined from the ac conductivity plots in the region of low-frequency plateau by fitting power law equation ($\sigma_{ac} = \sigma_{dc} + A\omega^n$, $0 < n < 1$).

Scanning electron microscopic (SEM) investigation was performed using FEI Quanta 200 on tensile fractured samples near the fracture surface after gold sputtering.

Differential scanning calorimetric (DSC) measurements were carried out using a Perkin–Elmer DSC-7 (Pyris software version 4.01). The extruded samples of about 5 mg were dried in a vacuum oven prior to experiment. The heating-cooling-heating cycles were recorded in the temperature range from −60 to 230°C at a scan rate of ±10 K/min under nitrogen atmosphere. Temperature and transition heat were calibrated with indium standard. In the 1st heating run all samples were annealed at the final temperature (230°C) for 0.5 min to delete the previous thermal history. The degree of crystallinity of PA12 phase was calculated from the heat of fusion of second heating run. The heat of fusion (ΔH_m) of PA12 phase was normalized to the fraction of PA12 present in the composites. The degree of crystallinity (X_c) of PA12 phase was determined from the ratio of normalized heat of fusion ($\Delta H_{m,\text{norm}}$) to the heat of fusion of 100% crystalline PA12, $(\Delta H_m)_0$, which was taken as 209.2 J/g.[25]

Wide-angle X-ray diffraction (WAXD) studies were carried out on a Philips X-Pert Pro. The incident X-rays (λ = 1.54 Å) from the Cu-target were monochromatized using a Ni filter. Compression molded samples of 0.35 mm thickness were used as test specimens. WAXD patterns were recorded in transmission mode with a step scan with step size of 0.02 between 2θ ranging from 5° to 40°.

Small angle X-ray scattering (SAXS) studies were carried out with threefold pinhole system (self-construction), main slit Ø = 100 μm with RIGAKU rotating anode operating at 40 kV and 100 mA utilizing Cu-K_α radiation (monochromatized by primary OSMIC confocal optic, focus radius 165 cm) in transmission mode.

RESULTS AND DISCUSSION

Interfacial interactions

It is one of the objectives of this study to modify the interfacial interaction between PA12 and SWNT in the presence of SMA copolymer. It is also assumed that the carbon nanotubes surface is encapsulated or covered at least partially by the SMA copolymer after the solvent removal while forming the ''mat'' structure of SMA modified SWNT. In this system, we have two interfaces: the one between the SWNT and the encapsulating SMA layer and the other one between the SMA layer and the matrix polyamide. After melt interfacial reaction between NH_2 end groups of PA12 and the anhydride groups of SMA, the later one may be shifted towards an interface between reacted PA12 chains at the SMA layer surface and the unreacted PA12 matrix.

Because of dispersive interactions between the aromatic groups of the styrene and the SWNT we expect that the copolymer is located and fixed at the SWNT surface physically by dispersive interactions. By this encapsulation one can expect a lower interfacial tension between PA12 and the SMA modified SWNT, which is indicated by comparing the surface tension data of CNT, PA12, and SMA copolymer available from the literatures. For MWNT, carbon nanofibers, and carbon fibers, Nuriel et al.[26] measured surface energies in the range of 40–45 mN/m, which is quite similar to untreated graphite fibers. We further assume that the surface tension of SWNT is in the same range. Polyamide 12 exhibits a surface tension of about 27 mN/m at 220°C.[27] For SMA 8 the surface tension at 220°C was determined to be 29.5 mN/m, whereas SMA14 shows a slightly higher value of 31 mN/m.[28] Thus, the encapsulation of the SWNT by a SMA layer minimizes the surface tension between PA12 and SWNT. On the other hand, the maleic anhydride groups are available for the interfacial reaction with the polyamide end groups during the melt mixing. The reaction is depicted schematically in Figure 2. This kind of interfacial reaction was selected to overcome the strong intertube van der Waals interaction, which is responsible for the persisting SWNT bundles in the composites even after application of high shear forces during

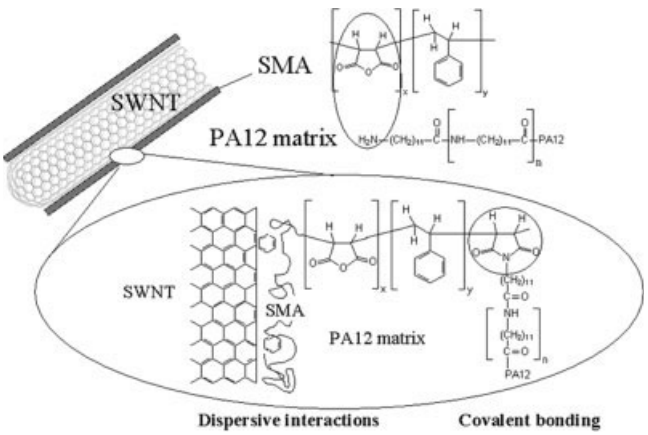

Figure 2 Schematic representation of the interfacial reaction between SMA and PA12.

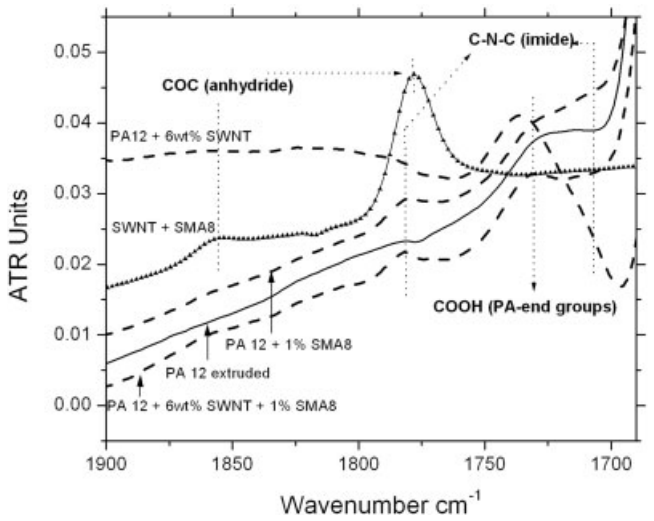

Figure 3 ATR spectra of different combinations (replotted with permission by Elsevier from Ref. 22).

melt mixing. The anhydride-amine reaction was shown in literature as one of the most effective reactions in obtaining finer morphology in polymer blends by reducing the interfacial tension between the two blend components.[29] It is very fast and can be accomplished within short melt mixing time and this reaction scheme was found to be suitable for our new approach and adapting it to polymer-filler interfaces.

The ATR spectra for different combinations are shown in Figure 3.[22] After wrapping SWNT with SMA the bands corresponding to the COC groups of the unreacted anhydride (ν_s = 1859 cm^{-1}, ν_{as} = 1782 cm^{-1}) are clearly visible. These bands are absent in PA12 and PA12/SWNT composites. The formation of imide groups (ν_s = 1785 cm^{-1}, ν_{as} = 1715 cm^{-1}) resulting from the reaction between the anhydride groups and the amine end groups of PA12 can be followed in the mixture of PA12 with 1 wt % SMA. In this case it represents a bulk reaction. The bands characteristic for the imide groups can also be observed in the composites with SMA wrapped SWNT, which is the manifestation of the reaction between the NH_2 end groups of PA12 and the anhydride groups of SMA.

Morphology of tensile fractured surfaces

The effect of SWNT addition and the modification of SWNT by encapsulation on the stress-strain behavior of the composites are intensively discussed in Ref. 22. When adding 3 or 6 wt % SWNT, tensile modulus, stress at yield and stress beyond the yield point increased significantly as compared to PA12 processed in the same way. For the 6 wt % SWNT sample, modulus increased by 40%, stress at yield by 20% and stress after yield point by 26%. On the other hand, elongation at break of the composites was reduced significantly. It decreased from ~500% for PA12 to ~150 and ~50%, for 3 and 6 wt % of SWNT respectively.[22] This behavior can be related to the formation of a percolated SWNT network, which is indicated by electrical conductivity measurements. Because of the existence of SWNT network, the polyamide matrix cannot perform its typical strain hardening behavior beyond the yield point and sample break occurs much earlier in the deformation process.

When adding SMA encapsulated SWNT, elongation at break could be partially brought back to higher values by retaining enhanced values in modulus and stresses at yield and beyond the yield point as compared to PA12. On the other hand we found that the samples were no longer conductive what we attribute to the encapsulating and insulating SMA layer/islands around the SWNT (see discussion dealing with electrical conductivity). We assume a superposition of facilitation of strain hardening induced by the polymer layer between geometrically connected SWNT and the better phase adhesion through the interfacial reaction. The weakest interface may be shifted from the SWNT/PA12 interface toward the interface between reacted PA12 chains at the SMA layer surface and the unreacted PA12 matrix. As shown later, significant changes in the degree of PA12 crystallinity can be excluded to be the reason for changed mechanical behavior.

We further investigated the tensile fractured surfaces by SEM to get more information about the state of SWNT dispersion, the encapsulation, and the interfacial adhesion. Figures 4–7 show the SEM micrographs of different composites. It was observed that all the samples exhibit the formation of shear bands (including PA12) in the crack-propagating zone. Figure 4 depicts the formation of shear bands exemplary for PA12/SWNT and PA12/3 wt % SWNT/1 wt % SMA14 composites, which is a manifestation of ductile failure.

SEM observations of the crack-initiation zone of the fractured samples reveal information about the SWNT dispersion (Fig. 5). Fractured surface of the composites with untreated SWNT [Fig. 5(a)] indicates the existence of areas with different SWNT density, which is due to less homogeneously dispersed SWNT aggregates. However, in case of modified SWNT homogeneously dispersed SWNT is observed in all the samples investigated, exemplary shown for the PA12/6 wt % SWNT/1 wt % SMA14 composite [Fig. 5(b)]. The fractured surface also displays the presence of smaller SWNT bundles as compared to unmodified SWNT.

Differences in the phase adhesion are shown in Figure 6. In case of unmodified SWNT, the tubes

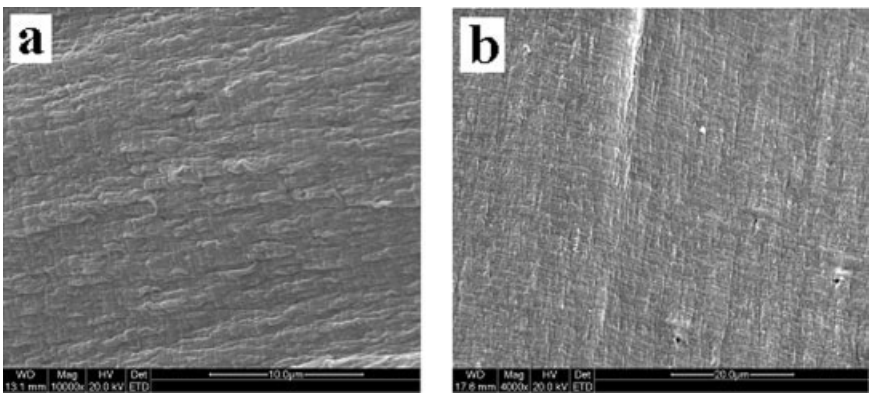

Figure 4 Shear bands formation in the tensile fractured surfaces of (a) PA12 + 3 wt % SWNT and (b) PA12 + SWNT (3 wt %) + SMA14 (1 wt %).

found to be pulled out from the matrix after the mechanical test and are only loosely adhered to the matrix [Fig. 6(a)]. In contrast, SMA modified tubes are well adhered to the matrix and are even seen to bridge a crack [Fig. 6(b)]. For this sample, the elongation at break was about three times of that with unmodified SWNT. The phenomenon of bridging a crack by SMA modified SWNT is once again manifested in Figure 7(a). Several micron long SWNT bundles stretch between two parts of the matrix. It can be assumed that the SMA encapsulated SWNT participated in the entire deformation process as indicated by the observation of stretched SWNT bundles in these composites. This also indicates the efficient load transfer during the deformation process due to the enhanced interfacial adhesion.

Next to the finding of smaller SWNT bundles after SMA modification, we also observed the effect of encapsulation, especially in crack bridging zones as shown in Figure 7(b). These bridging SWNT appear to be much thicker than SWNT in other areas of the sample. This is presumably the interfacial zone between the PA12 matrix and SWNT bundles adhered to a layer consisting of SMA and chemically bonded PA12 chains, which are especially visible in zones with high local stresses because of small cracks.

AC electrical conductivity of PA12/SWNT composites

The frequency dependence electrical conductivity at room temperature (20°C) for pure PA12, PA12/SWNT, and PA12/SWNT + SMA composites is depicted in Figure 8. The bulk conductivity of pure PA12 increases with frequency with a value of about 10^{-13} S/cm at 0.01 Hz, which is expected for insulating materials. PA12/SWNT composites with 3 wt % SWNT content show a frequency independent plateau (DC conductivity of $\sim 10^{-10}$ S/cm) up to a critical frequency (ω_c of $\sim$0.22 Hz) beyond which conductivity dispersion is observed. This is in accordance with the ''Johnscher Universal Power law'' for frequency dependent conductivity of solids.[30] Composites with 6 wt % SWNT exhibit a DC conductivity of $\sim 10^{-7}$ S/cm^{-1} and an increase in ω_c ($\sim$3625 Hz). The increase in conductivity in case of PA12/SWNT composites with 6 wt % SWNT content may

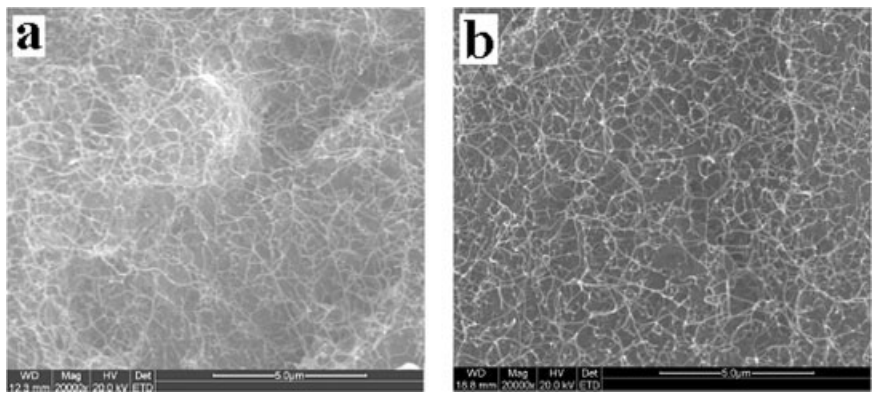

Figure 5 Tensile fractured surfaces of (a) PA12 + SWNT (6 wt %) and (b) PA12 + SWNT (6 wt %) + SMA14 (1 wt %) showing SWNT aggregation in (a) and finer dispersion in (b).

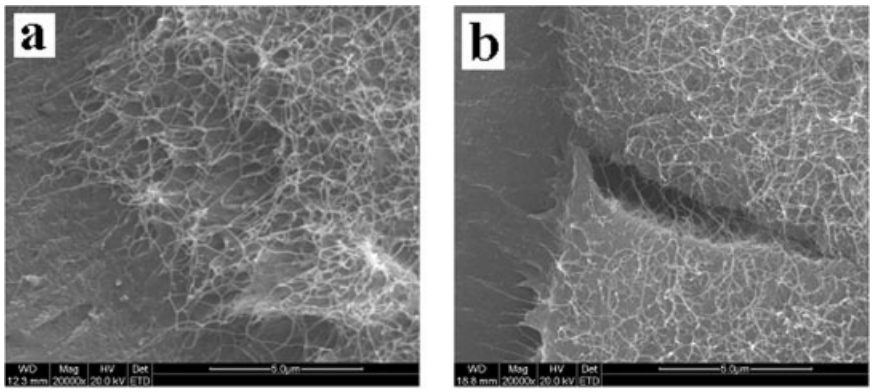

Figure 6 Tensile fractured surfaces of (a) PA12 + SWNT (6 wt %) and (b) PA12 + SWNT (6 wt %) + SMA14 (1 wt %) showing the inadequate interfacial adhesion in (a) and good interfacial adhesion in (b).

be due to ''network-like structure'' formation of SWNT. However, the absolute value of DC conductivity at this composition manifests the low purity level (55%) of SWNT used in this work along with the existence of SWNT bundles in the percolating network structure. Further, the electrical conductivity of PA12/SMA modified SWNT composites showed insulating behavior even at 6 wt % SWNT content. This observation can be attributed to encapsulated SMA copolymer layer on SWNT surface (see SEM micrographs) inhibiting electrical contacts between the tubes.

Crystalline morphology from DSC, WAXD, and SAXS

It is well known from literature, that carbon nanotubes act as nucleating agents by enhancing the crystallinity and the crystallization temperatures of the matrix polymer. Exemplarily such effects are described in Ref. 31 where a crystalline layer of poly (vinyl alcohol) formed around the nanotubes was shown to maximize interfacial stress transfer. Therefore, in connection with changes in mechanical properties it is also important to investigate the effect of SWNT addition on the crystallization behavior and crystalline morphology for our system.

Figure 9 shows the DSC melting endotherms of PA12 and the composites with 3 wt % SWNT. PA12 and the composite with SMA8 modified SWNT show a double melting endothermic peak in the second heating run, whereas the composites of PA12/SWNT and with SMA14 modified SWNT exhibit a single melting endothermic peak. The presence of double melting endothermic peak may be related to melting-recrystallization process or may be originated from mixed crystal structures, which will be discussed in the subsequent section related to WAXD analysis. The thermograms for the composites with 6 wt % SWNT showed the same qualitative behavior (not shown). It can be seen from Table I that the degree of crystallinity of PA12 only increases marginally on incorporation of either unmodified or SMA encapsulated SWNT for both concentrations. Slightly higher values are found for the composites with 6 wt % SMA modified SWNT as compared to 6 wt % unmodified SWNT. The crystalline melting temperature (T_m) of PA12 remains unchanged with addition of SWNT.

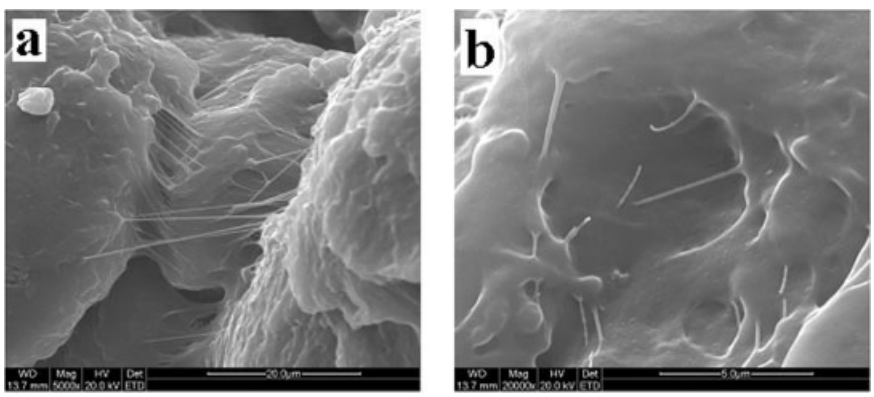

Figure 7 Tensile fractured surfaces of PA12 + SWNT (6 wt %) + SMA8 (1 wt %) showing the stretched SWNT bridging the cracks in (a) and tube breakage and polymer encapsulated SWNT in (b).

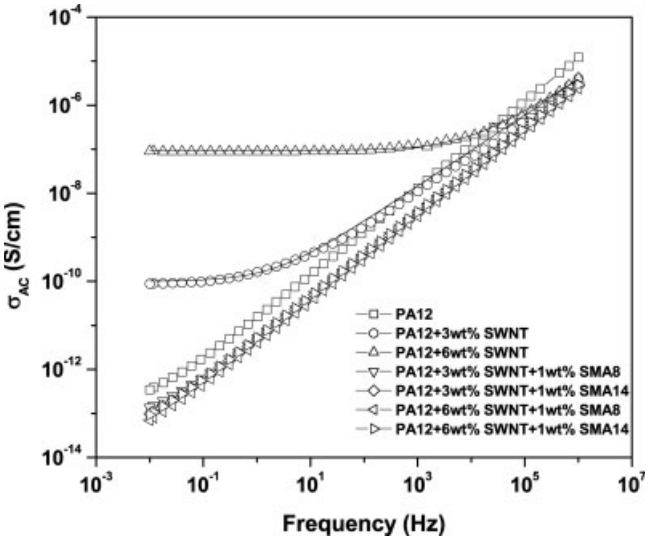

Figure 8 Frequency dependence AC conductivity of PA12/SWNT and PA12/SWNT + SMA composites.

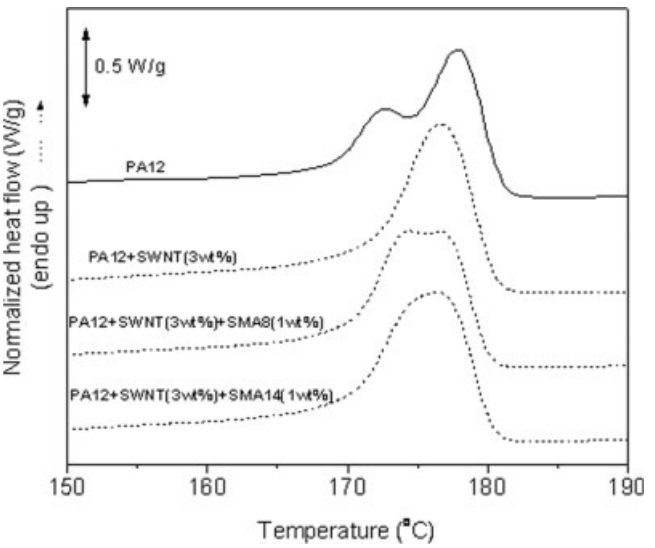

Figure 9 DSC melting endotherms of SMA modified PA12/SWNT composites.

Figure 10 shows the crystallization exotherms and indicates that both, unmodified and SMA modified SWNT, act as nucleating agents, since the crystallization temperature ($T_{c,m}$) and the onset temperature of nucleation ($T_{c,0}$) of PA12 increase by 4–6 K. This observation is consistent with the results reported for PP/SWNT and PA12/MWNT composites.[10,11] As discussed in *Morphology of tensile fractured surfaces*, the encapsulation of SWNT by SMA resulted in a finer dispersion of the SWNT in PA12 matrix. It was expected that this would lead to a higher population of nuclei at the early stages of crystallization and would affect the onset temperature of nucleation $T_{c,0}$ and the maximum crystallization temperature $T_{c,m}$ to a greater extent. On the contrary, the experimental results suggest that SMA modified SWNT act in a slightly lower magnitude than unmodified SWNT. This may be explained by counteracting effects of better dispersion leading to higher nanotube surface area and the formation of a copolymer layer or copolymer islands on the surface of SWNT bundles, leading to a decrease in free nanotube surface area available for nucleation. The findings that the nucleation effect as seen in $T_{c,0}$ and T_c are reduced, whereas dispersion of SWNT is enhanced serves as a clear indication that the SMA copolymer at least partially covers the SWNT surface.

Figure 11 shows the diffraction patterns obtained from wide angle X-ray diffraction analysis of PA12 and some of the composites. Pure PA12 usually crystallizes into the γ-crystalline form corresponding to 002, 004, and 001 reflection. In the diffraction pattern of PA12 the diffraction maxima is observed at $2\theta = 21.25^\circ$ (001 reflection) corresponding to d spacing of about 4.18 Å which is characteristic for the γ-crystalline form of PA12. In the composites with SWNT and SMA encapsulated SWNT the γ-crystalline form is also present and the *d* spacings remain unaltered. Analysis of the full width at half maximum (FWHM) of the crystalline peak reveals an increased crystallite size corresponding to the 001 reflection for PA12/SWNT and PA12/SWNT + SMA composites as indicated by a decreased FWHM value. The crystallite size corresponding to 001 reflection of PA12 was also calculated by the Debye Scherrer equation and was found to increase from 70.5 to 81–86 Å for PA12

TABLE I
Melting and Crystallization Parameters for PA12, PA12/SWNT, and PA12/SWNT + 1 wt % SMA Composites

Sample code	Compositions (wt %)			X_c (%)	T_m (°C)	$T_{c,m}$ (°C)	$T_{c,0}$ (°C)
	PA12	SWNT	SMA				
PA12	100	0	0	34.2	172.6/177.8	151.7	155.0
PA12 + 3SWNT	97	3	0	34.6	176.6	157.9	161.5
PA12 + 6SWNT	94	6	0	34.8	176.2	158.1	161.8
PA12 + 3SWNT + SMA8	96	3	1	34.4	174.4/176.6	156.2	159.3
PA12 + 3SWNT + SMA14	96	3	1	35.1	176.4	155.8	159.0
PA12 + 6SWNT + SMA8	93	6	1	35.9	174.8/176.8	156.2	159.3
PA12 + 6SWNT + SMA14	93	6	1	36.4	175.6	156.2	159.4

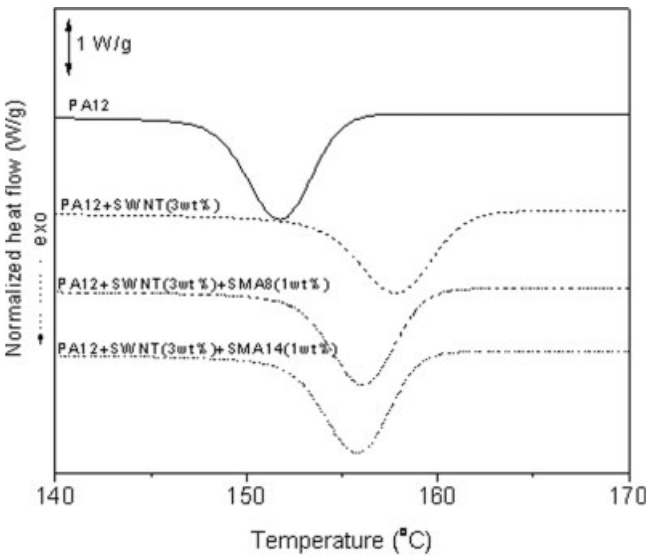

Figure 10 DSC crystallization exotherms of SMA modified PA12/SWNT composites.

composites with SWNT and SMA modified SWNT. This can be explained in terms of heteronucleation effect of the nanofillers; early nucleation leaves more space for the heteronucleated crystals to grow, before homogeneous nucleation within the remaining part of the matrix leads to impingement.[11]

Figure 12 shows the Lorentz corrected SAXS plot of Iq^2 versus q, where I is the intensity and q is the scattering vector (= $2\pi/d$), the maxima of the peak corresponds to the long period (L_w) obeying the relationship $L_w = 2\pi/q$. It can be seen that the long period of PA12 increases from 79.4 to 102.9 Å in case of SMA modified PA12/SWNT (6 wt %) composites. The other SMA modified compositions as well show an increase of the long period of PA12.

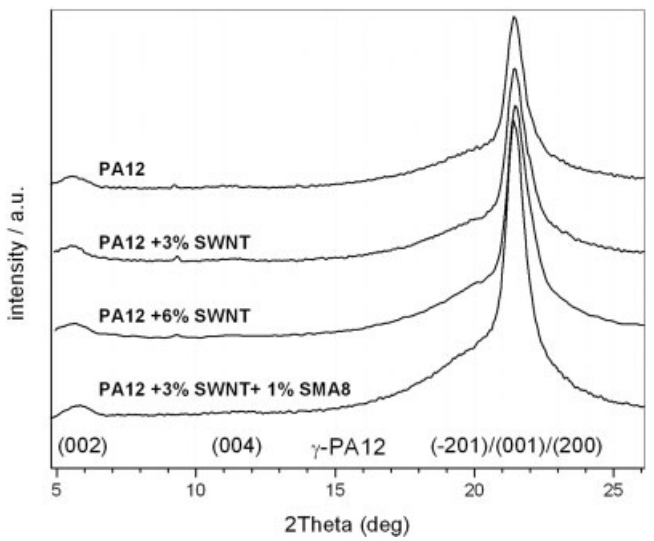

Figure 11 WAXD of PA12 and PA12/SWNT composites.

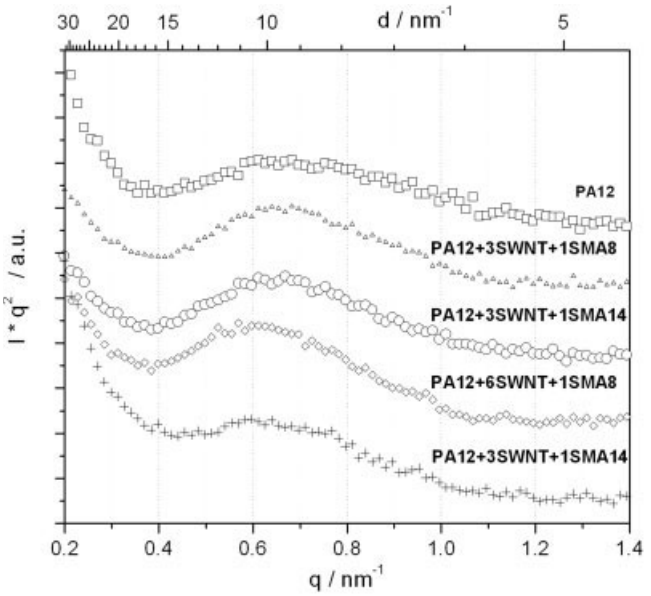

Figure 12 Lorentz corrected SAXS plot of Iq^2 versus q, where I is the intensity and q is the scattering vector.

The calculation of the crystalline lamella thickness (L_c) and amorphous interlayer thickness (L_a) revealed an increase of L_c and L_a of PA12 in SMA modified SWNT composites. The increase in L_a indicates the presence of SMA modified SWNT in the amorphous phase of PA12 due to the interfacial reaction as discussed in the earlier section. While accommodating SMA chains in the amorphous interlayer regions of PA12, it is most likely that there would be delay in the crystallization process of PA12 and the crystals will get enough time to grow manifesting in increase in L_c even if the presence of partially covered SWNT are acting as heterogeneous nucleation sites. The increase in L_c may be due to crystal thickening and is found to be consistent with WAXD results related to the larger crystal size of PA12.

SUMMARY AND CONCLUSIONS

Single wall carbon nanotubes (SWNT) encapsulated by styrene maleic anhydride copolymer (SMA) were melt-mixed with polyamide 12 (PA12) utilizing the concept of reactive compatibilization. In particular, an interfacial reaction between the anhydride functionality of SMA and the amine end groups of PA12 was used.

This reaction could be proven by ATR-FTIR spectroscopy. Because of this interfacial reaction, an enhancement of the interfacial adhesion between PA12 and SMA modified SWNT was observed from microscopic investigations of the tensile fractured morphology of the composites. It may also be expected that the nanotube network structure is much more stable against reaggregation of CNT

during further processing when reactively coupled with the matrix phase. Electrical conductivity measurements reveal the formation of percolating network at 6 wt % SWNT content in PA12/SWNT composites, however, the SMA modification used led to an impingement in the geometrically connected SWNT network in PA12/SWNT + SMA composites. In general, it can be concluded that SMA encapsulation of SWNT provides a partial wrapping of a polymer layer (SMA and reactively coupled PA12) on SWNT bundles, which is evident from SEM observation and electrical conductivity measurements.

DSC investigations indicated the nucleating action of unmodified and SMA encapsulated SWNT in the respective composites as found from the increase in the crystallization temperature. However, the extent of nucleating action as seen in $T_{c,0}$ and T_c of SMA encapsulated SWNT is found to be less as compared to unmodified SWNT which can be related to the encapsulating SMA layer/islands around the SWNT. In addition, it also indicated that the remaining portion of the free nanotube surface aids in nucleation for PA12 crystallization.

The overall crystallinity of PA12 remained unchanged in case of 3 wt % modified SWNT and was only marginally increased in case of 6 wt % modified SWNT. In addition, changes in the crystalline morphology of PA12 were observed from WAXD and SAXS. In particular, an increase in PA12 crystallite size, crystalline lamella thickness and the amorphous interlayer thickness in the presence of SWNT and SMA modified SWNT were found.

In summary, the results showed the applicability of the selected compatibilization route. They indicate interplay between better dispersion, enhanced interphase adhesion, enhanced crystallization behavior and partial SWNT wrapping by the compatibilizer. Thus, to apply the concept successfully in practical application, a good balance in partial covering of SWNT surfaces by the compatibilizer is required. By this way, retaining conductivity as well as enhancing mechanical properties can be expected. This should be achieved by selecting a suitable compatibilizer, balancing the amount and reactivity of the compatibilizer in relation to the CNT content used and should be the task of future investigations.

We thank Nanoledge Inc. (France) for providing PA12 and SWNT. In addition, we are grateful to Carmen Bunescu (Forschungszentrum Wismar e.V., Germany) for TEM of the SWNT, to Vivek Pancholi (OIM-SEM National Facility, IIT Bombay) for assistance in SEM investigation, and to Prof. Raman S. Srinivasa (Metallurgical Engineering and Materials Science, IIT Bombay) for useful discussions regarding WAXD measurements.

References

1. Iijima, S. Nature 1991, 354, 56.
2. Salvetat, J. P.; Briggs, G. A. D.; Bonard, J. M.; Bacsa, R. R.; Kulik, A. J.; Stöckli, T.; Burnham, N. A.; Forró, L. Phys Rev Lett 1999, 82, 944.
3. Dresselhaus, M. S.; Dresselhaus, G.; Avouris, Ph. Carbon Nanotubes: Synthesis, Structure, Properties, and Applications; Springer-Verlag: Germany, 2001.
4. Kumar, S.; Dang, T. D.; Arnold, F. E.; Bhattacharyya, A. R.; Min, B. G.; Zhang, X.; Vaia, R. A.; Park, C.; Adams, W. W.; Hauge, R. H.; Smalley, R. E.; Ramesh, S.; Willis, P. Macromolecules 2002, 35, 9039.
5. Shaffer, M. S. P.; Windle, A. H. Adv Mater 1999, 11, 937.
6. Schadler, L. S.; Giannaris, S. C.; Ajayan, P. M. Appl Phys Lett 1998, 73, 3842.
7. Sandler, J.; Shaffer, M. S. P.; Prasse, T.; Bauhofer, W.; Schulte, K.; Windle, A. H. Polymer 1999, 40, 5967.
8. Valentini, L.; Biagiotti, J.; Kenny, J. M.; Santucci, S. J Appl Polym Sci 2003, 87, 708.
9. Grady, B. P.; Pompeo, F.; Shambaugh, R. L.; Resasco, D. E. J Phys Chem B 2002, 106, 5852.
10. Bhattacharyya, A. R.; Sreekumar, T. V.; Liu, T.; Kumar, S.; Ericson, L. M.; Hauge, R. H.; Smalley, R. E. Polymer 2003, 44, 2373.
11. Sandler, J. K. W.; Pegel, S.; Cadek, M.; Gojny, F.; van Es, M.; Lohmer, J.; Blau, W. J.; Schulte, K.; Windle, A. H.; Shaffer, M. S. P. Polymer 2004, 45, 2001.
12. Cadek, M.; Coleman, J. N.; Ryan, K. P.; Nicolosi, V.; Bister, G.; Fonseca, A.; Nagy, J. B.; Szostak, K.; Beguin, F.; Blau, W. J. Nano Lett 2004, 4, 353.
13. Gong, X.; Liu, J.; Baskaran, S.; Voise, R. D.; Young, J. S. Chem Mater 2000, 2, 1049.
14. Barrau, S.; Demont, P.; Perez, E.; Peigney, A.; Laurent, C.; Lacabanne, C. Macromolecules 2003, 36, 9678.
15. Mitchell, C. A.; Bahr, J. L.; Arepalli, S.; Tour, J. M.; Krishanamoorti, R. Macromolecules 2002, 35, 8825.
16. Velasco-S. C.; Martinez-H, A. L.; Fisher, F. T.; Ruoff, R.; Castano, V. M. Chem Mater 2003, 15, 4470.
17. Zhang, W. D.; Shen, L.; Phang, I. Y.; Liu, T. Macromolecules 2004, 37, 256.
18. Liu, T.; Phang, I. Y.; Shen, L.; Chow, S. Y.; Zhang, W. D. Macromolecules 2004, 37, 7214.
19. Kodgire, P. V.; Bhattacharyya, A. R.; Bose, S.; Gupta, N.; Kulkarni, A. R.; Misra, A. Chem Phys Lett 2006, 432, 480.
20. Xia, H.; Wang, Q.; Qiu, G. Chem Mater 2003, 15, 3879.
21. Bellayer, S.; Gilman, J. W.; Eidelman, N.; Bourbigot, S.; Flambard, X.; Fox, D. M.; De Long, H. C.; Trulove, P. C. Adv Funct Mater 2005, 15, 910.
22. Bhattacharyya, A. R.; Pötschke, P.; Abdel-Goad, M.; Fischer, D. Chem Phys Lett 2004, 392, 28.
23. Bhattacharyya, A. R.; Pötschke, P.; Häußler, L.; Fischer, D. Macromol Chem Phys 2005, 206, 2084.
24. Bhattacharyya, A. R.; Pötschke, P. Macromol Symp 2006, 233, 161.
25. McNally, T.; Murphy, W. R.; Lew, C. Y.; Turner, R. J.; Brennan, G. P. Polymer 2003, 44, 2761.
26. Nuriel, S.; Liu, L.; Barber, A. H.; Wagner, H. D. Chem Phys Lett 2005, 404, 263.
27. http://www.surface-tension.de/solid-surface-energy.htm. Accessed on 28 October, 2005.
28. Pionteck, J.; Kreßler, J. In Europhysics Conference Abstracts; Pick, R., Ed.; The European Physical Society: EPFL, Lausanne, Switzerland, 1997; Vol. 21B, p 31.
29. Sundararaj, U.; Macosko, C. W. Macromolecules 1995, 28, 2647.
30. Jonscher, A. K. Nature 1977, 267, 673.
31. Coleman, J. N.; Cadek, M.; Blake, R.; Nicolosi, V.; Ryan, K. P.; Belton, C.; Fonseca, A.; Nagy, J. B.; Gunko, Y. K.; Blau, W. J. Adv Funct Mater 2004, 14, 791.